JMEPEG (2009) 18:649–654
DOI: 10.1007/s11665-009-9409-7

1059-9495/$19.00

SMA Numerical Modeling Versus Experimental Results: Parameter Identification and Model Prediction Capabilities

Ferdinando Auricchio, Alberto Coda, Alessandro Reali, and Marco Urbano

(Submitted October 14, 2008; in revised form January 17, 2009)

In this work, we briefly review the one-dimensional version of a well-known phenomenological shape memory alloy (SMA) constitutive model able to represent the main macroscopic SMA macroscopic behaviors (i.e., superelasticity and shape-memory effect). We then show how to identify the needed parameters from experimental results and, in particular, from strain-temperature tests. We finally use the obtained material parameters to test the prediction properties of the model, comparing numerical results with some experiments (different from those used for the identification), and we discuss model capabilities and further required enhancements.

Keywords experimental results, numerical modeling, parameter identification, shape memory alloys

1. Introduction

The research toward an exhaustive modeling of the macroscopic behavior of shape memory alloys (SMAs) has been widely growing in last years because of the increasing employment of such smart materials in a large number of applications in many fields of engineering.

Thus, many models able to reproduce SMA main macroscopic effects have been recently proposed in the literature in one or in three dimensions (see, e.g., Ref 1-8).

The purpose of such works is to give reliable models which could be used by engineers who need to perform accurate simulations to design and study the response of SMA structures or components. To reach this goal, the proposed models have to be interfaced with analysis programs which are commonly used in engineering offices during the design process of a real device; accordingly, a good model should also be robust and flexible, possibly including both superelasticity and shape-memory effect, without becoming too complex. Also, the problem of the physical interpretation of the model parameters is an important issue, as a clear and effective parameter identification procedure is the key for the employment of a constitutive model by engineers in real-life simulations.

Among the different models available in the recent literature, the one introduced in Ref 9 and improved in Ref 10 seems to be very attractive. Developed within the theory of irreversible thermodynamics, this model is in fact able to describe both superelasticity and shape-memory effect (see Fig. 1), and the corresponding solution algorithm is simple and robust as it is based on a plasticity-like return map procedure. Its robustness makes the model particularly suitable for implementation within finite element codes, allowing the simulation of the behavior of complex SMA devices.

In the following, we focus on the 1D model obtained by the reduction of the 3D model described in Ref 10. We briefly show and comment the basic equations, as well as the physical meaning and a possible identification strategy for the needed material parameters. We then show the application of the proposed procedure in order to simulate the behavior of a SMA wire, comparing our numerical results with experimental tests.

2. Basic Model Equations

The model equations arise from a free energy density function Ψ defined as

$$\Psi(\varepsilon, \varepsilon^{\mathrm{tr}}, T) = \frac{1}{2}E(\varepsilon - \varepsilon^{\mathrm{tr}})^2 + \tau_{\mathrm{m}}(T)|\varepsilon^{\mathrm{tr}}| + \frac{1}{2}h(\varepsilon^{\mathrm{tr}})^2 + I_{\varepsilon_{\mathrm{L}}}(\varepsilon^{\mathrm{tr}}),$$

where the physical meaning of the different material parameters are discussed in the next section. To satisfy the transformation strain constraint $|\varepsilon^{\mathrm{tr}}| \leq \varepsilon_{\mathrm{L}}$, the indicator function $I_{\varepsilon_{\mathrm{L}}}(\varepsilon^{\mathrm{tr}})$ is used, which is defined as

$$I_{\varepsilon_{\mathrm{L}}}(\varepsilon^{\mathrm{tr}}) = \begin{cases} 0 & \text{if } |\varepsilon^{\mathrm{tr}}| \leq \varepsilon_{\mathrm{L}}, \\ +\infty & \text{otherwise.} \end{cases}$$

This article is an invited paper selected from presentations at Shape Memory and Superelastic Technologies 2008, held September 21-25, 2008, in Stresa, Italy, and has been expanded from the original presentation.

Ferdinando Auricchio and **Alessandro Reali**, Dipartimento di Meccanica Strutturale, Università degli Studi di Pavia, Pavia, Italy, European Centre for Training and Research in Earthquake Engineering (EUCENTRE), Pavia, Italy, and Istituto di Matematica Applicata e Tecnologie Informatiche (IMATI), CNR, Pavia, Italy; and **Alberto Coda** and **Marco Urbano**, SAES Getters Group, Lainate, MI, Italy. Contact e-mail: auricchio@unipv.it.

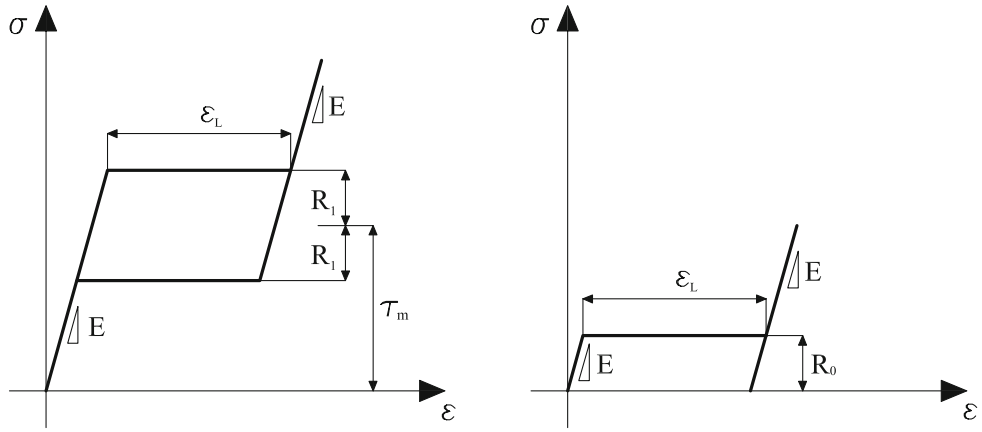

Fig. 1 Superelastic effect (*left*) and shape-memory effect (*right*). Graphical representation for the material parameters required by the constitutive model

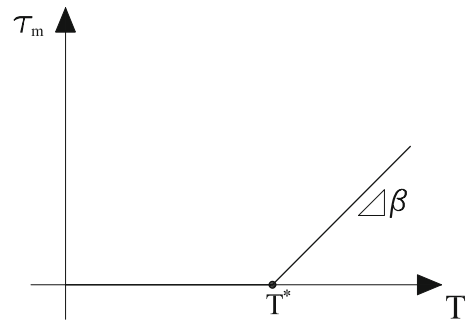

Fig. 2 Temperature dependence for τ_m

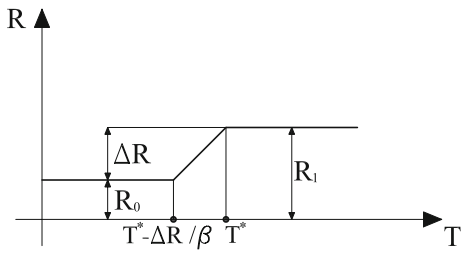

Fig. 3 Temperature dependence for the elastic domain radius R

Moreover, the dependence of τ_m on temperature (depicted in Fig. 2) is expressed as

$$\tau_m(T) = \beta(T - T^*)^+,$$

where the positive part function is defined as $(a)^+ = (a + |a|)/2$. The constitutive equations for the model are then classically obtained as follows:

$$\begin{cases} \sigma = \frac{\partial \Psi}{\partial \varepsilon} = E(\varepsilon - \varepsilon^{tr}), \\ X = -\frac{\partial \Psi}{\partial \varepsilon^{tr}} = \sigma - \tau_m(T)\frac{\varepsilon^{tr}}{|\varepsilon^{tr}|} - h\varepsilon^{tr} - \gamma\frac{\varepsilon^{tr}}{|\varepsilon^{tr}|}, \end{cases}$$

where X is the thermodynamic stress-like quantity associated to the transformation strain ε^{tr}. The variable γ results from the (sub)differentiation of the indicator function and fulfills

$$\begin{cases} \gamma = 0 \quad \text{if } |\varepsilon^{tr}| < \varepsilon_L, \\ \gamma \geq 0 \quad \text{if } |\varepsilon^{tr}| = \varepsilon_L. \end{cases}$$

To control the evolution of the internal variable ε^{tr}, a limit function F is introduced and is defined as

$$F(X) = |X| - R(T),$$

where the radius of the elastic domain $R(T)$ controls the width of the hysteresis loops (its dependence on temperature is illustrated in Fig. 3).

Considering then an associative framework, the flow rule for the internal variable takes the form

$$\dot{\varepsilon}^{tr} = \dot{\zeta}\frac{\partial F}{\partial X} = \dot{\zeta}\frac{X}{|X|}.$$

The model is finally completed by the classical Kuhn-Tucker conditions

$$\begin{cases} \dot{\zeta} \geq 0, \\ F \leq 0, \\ \dot{\zeta}F = 0. \end{cases}$$

3. Model Input Material Parameters

As seen from the equations introduced in the previous section, the 1D model requires eight material parameters indicated as E, ε_L, h, R_0, R_1, β, T^*, and δ.

A brief description along with some comments on such parameters follows:

- E: elastic modulus.
  In this model, the same elastic modulus for austenite and martensite is assumed. Different moduli for the two phases will be accounted for in future developments.
- ε_L: maximum transformation strain.
  This material constant measures the maximum strain obtainable through alignment of the martensite variants.
- h: stress-strain slope measure during transformation.
  This material constant is important in measuring the slope of the stress-strain diagram during the transformation, in fact $\frac{\partial \sigma}{\partial \varepsilon} = \frac{Eh}{E+h}$ (h can be interpreted as a standard linear kinematic hardening parameter, as in classical elasto-plastic models). Note that $\frac{\partial \sigma}{\partial \varepsilon} = \frac{Eh}{E+h} \simeq h$ when $E \gg h$. In particular, for $h = 0$ the stress-strain diagram shows a flat plateau (as in Fig. 1).

- R_0: elastic domain radius at low temperatures.
- R_1: elastic domain radius at high temperatures.
  To match the different radii with temperature, we assume a dependence of R on T as described in Fig. 3. In particular, R_0 is equal to half of the hysteresis loop width at low temperatures. R_1, instead, is equal to half of the hysteresis loop width at high temperatures, i.e. for $T > T^*$.
- β: slope of τ_m (see Section 2 and Fig. 1) with respect to temperature, as represented in Fig. 2.
- T^*: reference temperature, important in defining the dependence of τ_m on temperature (see again Fig. 2).

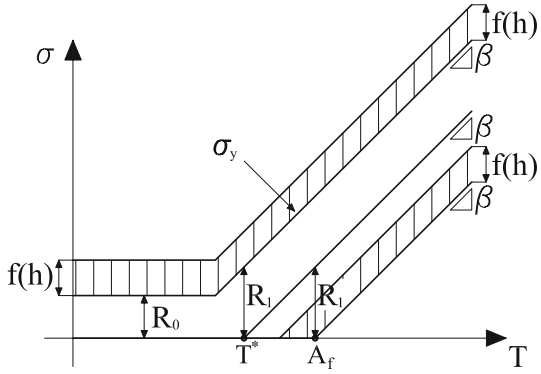

Fig. 4 Temperature dependence for the transformation stress σ_y. $f(h) = \frac{Eh}{E+h}\varepsilon_L$, and, when $E \gg h$, $f(h) \simeq h\varepsilon_L$

Moreover, β and T^* are also important in expressing the dependence on temperature of the transformation stress $\sigma_y = \tau_m + R$ (see Fig. 4). In particular, β represents the slope of σ_y with respect to temperature.

- δ: regularization parameter.
  To guarantee numerical solvability, a regularization is performed on the norm of the transformation strain as follows:

$$\overline{|\varepsilon^{tr}|} = \sqrt{(\varepsilon^{tr})^2 + \delta} - \sqrt{\delta},$$

  where δ is a small (e.g., $\sim 10^{-8}$) user-defined regularization parameter.

4. Model Response to Simple Test Situations

The most common situations that can be encountered in standard tests at constant temperature or stress are here considered and explained, also through graphical representations (see Fig. 5-7).

In particular, in Fig. 5, a superelastic test at a constant temperature $T = T_{SE} > T^*$ is described. The test starts at $\sigma = 0$ and a loading phase is followed by an unloading phase up again to $\sigma = 0$. No residual strain is observed.

In Fig. 6, instead, a shape-memory test at a constant temperature $T = T_{SME} < T^*$ is described. The test starts at $\sigma = 0$ and a loading phase is followed by an unloading phase up again to $\sigma = 0$. In this case, a residual strain is observed (that can be, however, recovered by heating the material).

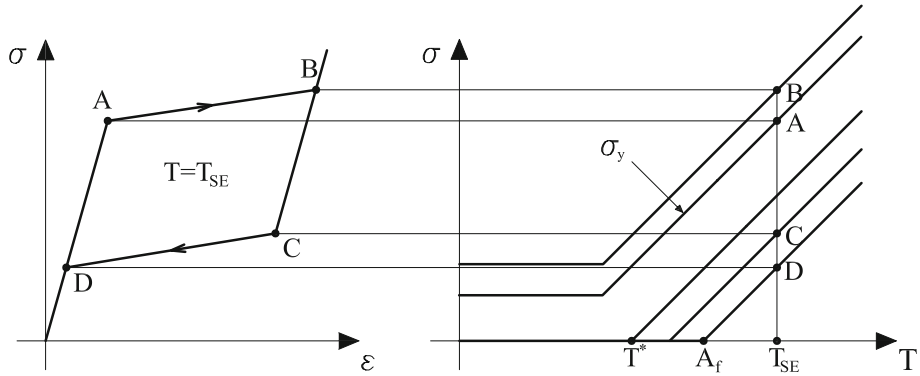

Fig. 5 Superelastic test (at a constant temperature $T = T_{SE}$): stress-strain diagram (*left*) and stress-temperature diagram (*right*)

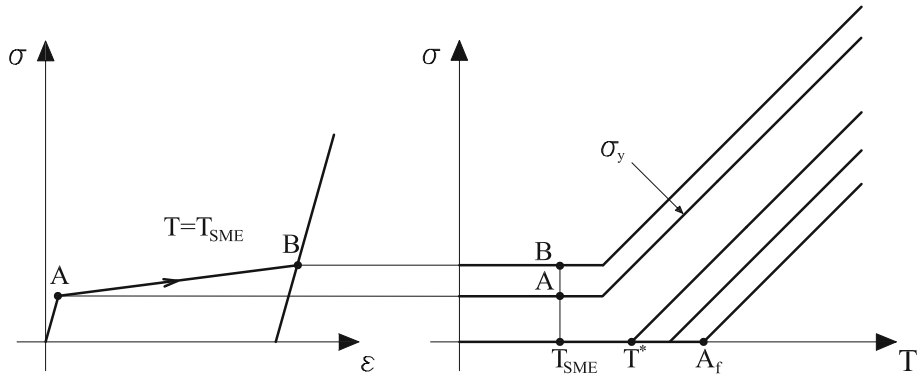

Fig. 6 Shape-memory test (at a constant temperature $T = T_{SME}$): stress-strain diagram (*left*) and stress-temperature diagram (*right*)

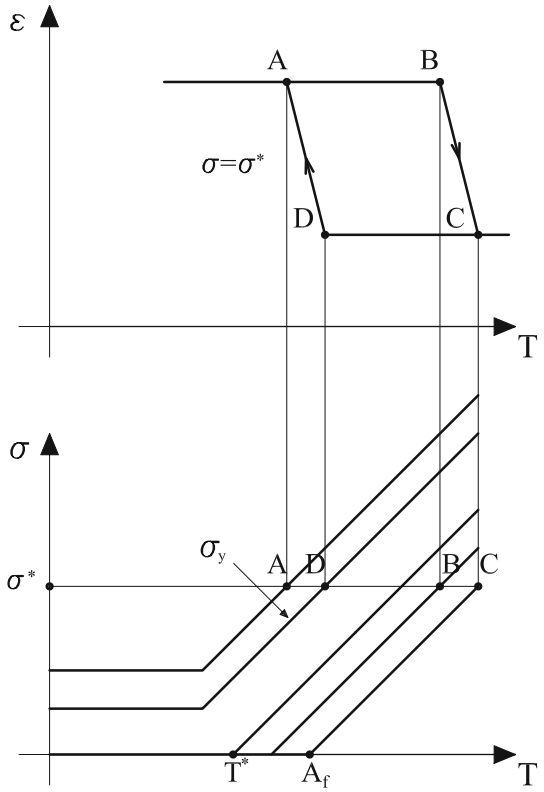

Fig. 7 $\varepsilon - T$ test (at a constant stress $\sigma = \sigma^*$): strain-temperature diagram (*top*) and stress-temperature diagram (*bottom*)

Finally, in Fig. 7, a strain-temperature test at a constant stress $\sigma = \sigma^*$ is described. The test starts at a low temperature (with the material at a stress level such that only martensite is present) and a heating phase is followed by a cooling phase up to the initial temperature.

5. Parameter Identification from a ε–*T* Test

Given two strain-temperature curves obtained at two constant stresses $\sigma^1 > \sigma^2$, as represented in Fig. 8, it is possible to identify in a simple way for all the needed material parameters.

In fact, as highlighted in the figure, ε_L is immediately obtained as the difference between the maximum and the minimum strain. E and β can be computed, using their definition, respectively, as

$$E = \frac{\Delta\sigma}{\Delta\varepsilon} \quad \text{and} \quad \beta = \frac{\Delta\sigma}{\Delta T},$$

with $\Delta\varepsilon$, $\Delta T = T^1_{yM} - T^2_{yM}$ and $\Delta\sigma = \sigma^1 - \sigma^2$ as indicated in the figure.

Then, it is possible to compute R_1 knowing that the hysteresis width is $2R_1/\beta$ (see again Fig. 8). The equation $T^1_{yA} - T^1_{yM} = 2R_1/\beta$ is obtained subtracting the two following equations (deriving from $F = |X| - R = 0$)

$$\begin{cases} \sigma - \beta(T_{yM} - T^*) = R_1, \\ \sigma - \beta(T_{yA} - T^*) = R_1. \end{cases}$$

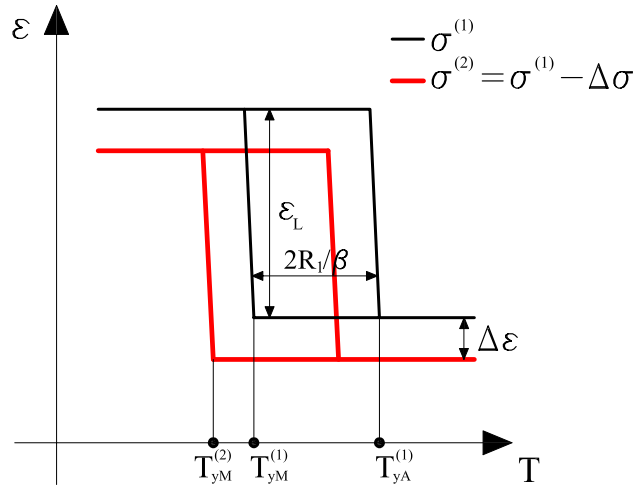

Fig. 8 Two strain-temperature curves at two constant stresses $\sigma^1 > \sigma^2$

Moreover, starting from $\frac{\partial\sigma}{\partial\varepsilon} = \frac{Eh}{E+h}$ and considering the dependence of the stress on temperature $\frac{\partial\sigma}{\partial\varepsilon} = \frac{\partial\sigma}{\partial T}\frac{\partial T}{\partial\varepsilon} = \beta\frac{\partial T}{\partial\varepsilon}$, with simple computations it can be found that

$$h = \frac{1}{\frac{1}{\beta}\frac{\partial\varepsilon}{\partial T} - \frac{1}{E}}.$$

Finally, to compute T^*, the following expression, directly derived from $\sigma^1 - \beta(T^1_{yM} - T^*) = R_1$, can be used

$$T^* = T^1_{yM} + \frac{R_1 - \sigma^1}{\beta}.$$

Alternatively, T^* could be computed from

$$T^* = A_f - \frac{R_1}{\beta},$$

as illustrated in Fig. 4. In this case, the austenite finishing temperature A_f is needed (and it may be obtained, e.g., from a differential scanning calorimetry, DSC).

6. An Example of Parameter Identification From a ε–*T* Test: Numerical Versus Experimental Results

In this section, an example of parameter identification (and numerical simulation) from a ε-*T* test is illustrated. We remark that we choose to use this kind of experimental results, instead of classical σ-ε curves, because the ε-*T* response is very significant for SMA producers, being one of the most important characteristic of SMA for actuators.

The experimental data (provided by the SAES Getters Group) shown in Fig. 9 and 10 have been obtained testing 0.2 mm NiTi wires at different temperatures, keeping the stress constant (in these examples, strain-temperature cycles at 100, 150, and 200 MPa are considered). It is to be remarked that here, instead of the strain ε, the "stroke" (referred to zero) is considered, i.e. for each "ε-*T*" curve the actual ordinate is $-(\varepsilon - \varepsilon_{min})$.

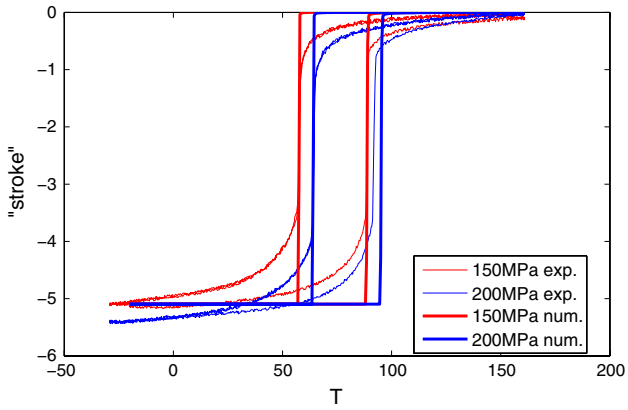

Fig. 9 Comparison of experimentally and numerically obtained curves relative to 0.2 mm wires at 150 and 200 MPa; the numerical curve at 150 MPa is fully fitted, while the one at 200 MPa is partially fitted and partially predicted

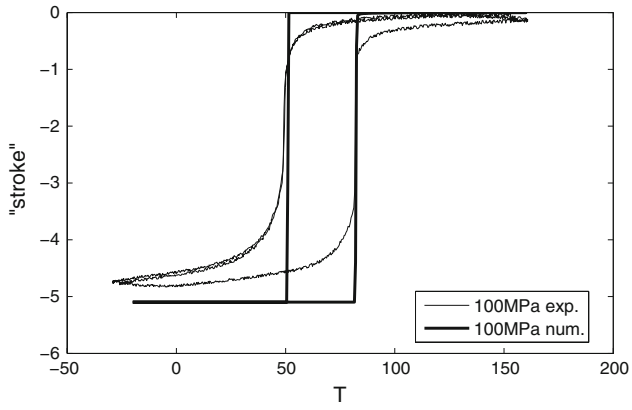

Fig. 10 Comparison of experimentally and numerically obtained curves relative to 0.2 mm wires at 100 MPa; the numerical curve is fully predicted

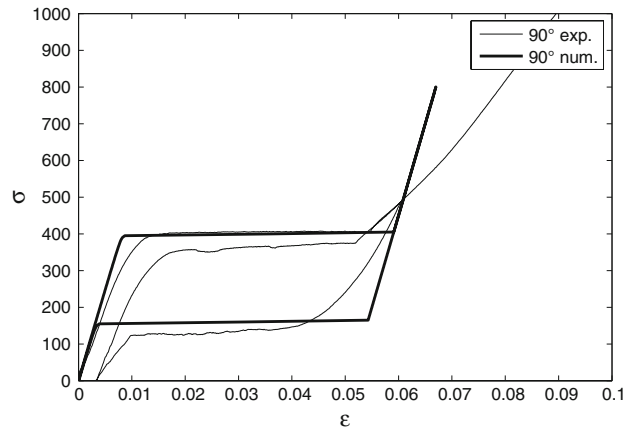

Fig. 11 Stress-strain tests at the temperature of 90 °C; the numerical curve is fully predicted (i.e., no curve fitting at all)

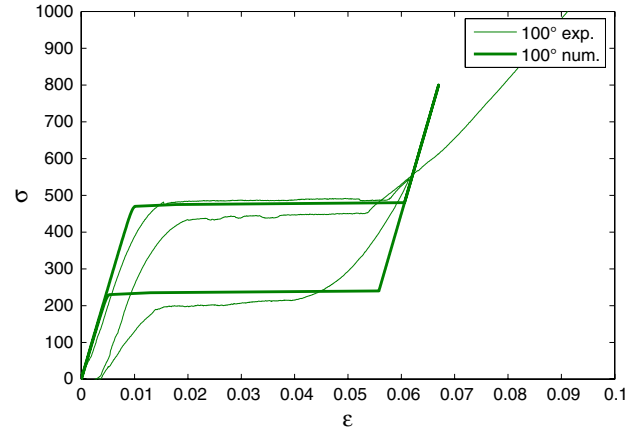

Fig. 12 Stress-strain tests at the temperature of 100 °C; the numerical curve is fully predicted (i.e., no curve fitting at all)

Performing the parameter identification procedure discussed in the previous section, the following set of material parameters has been obtained:

$$E = 50000 \text{ MPa}$$
$$\varepsilon_L = 5.1\%$$
$$h = 100 \text{ MPa}$$
$$R_0 = 40 \text{ MPa}$$
$$R_1 = 120 \text{ MPa}$$
$$\beta = 7.7 \text{ MPa}/^\circ\text{C}$$
$$T^* = 54 \,^\circ\text{C}$$
$$\delta = 10^{-8}$$

For the identification procedure, the 150 MPa curve has been used to compute ε_L and T^*, and, for the other parameters, the 150 and 200 MPa curves have been employed. Moreover, R_0 has been assumed to be smaller than 50 MPa (i.e., 40 MPa) as it has been experimentally observed that a hysteresis is present even at 50 MPa.

With these parameters, numerical curves have been produced and those for the 150 and 200 MPa cases are reported in Fig. 9 in order to compare them with the experimental ones from which the parameters have been identified. Moreover, Fig. 10 shows that a good agreement is obtained also for the 100 MPa curve, which has not been used for the identification procedure.

It is also to be remarked that in all these results an important role is played by the fact that in the model considered, at the moment, there is no distinction between the elastic moduli for austenite and martensite. This, in fact, makes constant the gap between the maximum and the minimum strain, while in the experimental results significant differences are observed.

Finally, some stress-strain tests at temperatures of 90, 100, 110, and 120 °C have been performed using the parameters computed above, and they have been compared with experimental data. The results are reported in Fig. 11-14, where a good agreement is observed in all cases.

7. Conclusions and Future Developments

In this work, we have considered the 1D version of the phenomenological SMA constitutive model presented in Ref 10

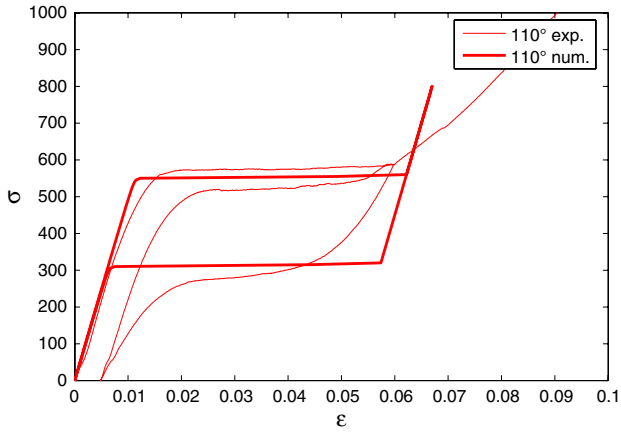

Fig. 13 Stress-strain tests at the temperature of 110 °C; the numerical curve is fully predicted (i.e., no curve fitting at all)

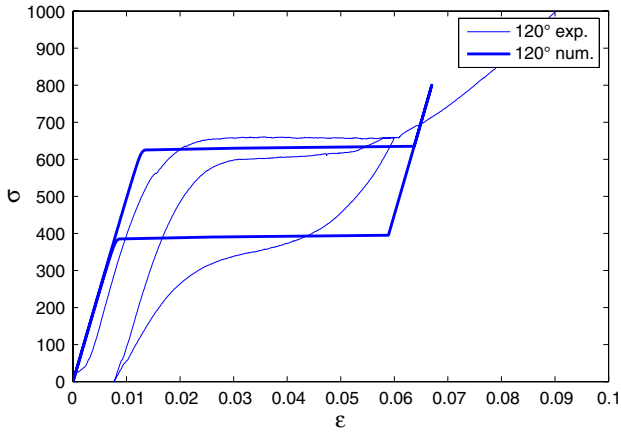

Fig. 14 Stress-strain tests at the temperature of 120 °C; the numerical curve is fully predicted (i.e., no curve fitting at all)

and, after a review of the model including a description of all the material parameters, we have shown a strategy to identify those parameters from experimental results and, in particular, from strain-temperature tests. We have then used such a procedure to obtain the material parameters for a real SMA wire in order to test the prediction properties of the model, comparing numerical results with some experiments (different from those used for identification) and obtaining a good agreement.

Finally, we remark that interesting extensions of the model, in order to have an even more accurate response, could be the implementation of:

- elastic properties depending on the transformation strain level (see Ref 11);
- plasticity and training effects (see Ref 12, 13);
- tension-compression asymmetries (see Ref 11); and
- fully coupled electric-thermo-mechanical analyses (see Ref 14).

References

1. S. Govindjee and C. Miehe, A Multi-Variant Martensitic Phase Transformation Model: Formulation and Numerical Implementation, *Comput. Methods Appl. Mech. Eng.*, 2001, **191**, p 215–238
2. D. Helm and P. Haupt, Shape Memory Behaviour: Modelling within Continuum Thermomechanics, *Int. J. Solids Struct.*, 2003, **40**, p 827–849
3. D.C. Lagoudas, P.B. Entchev, P. Popov, E. Patoor, L.C. Brinson, and X. Gao, Shape Memory Alloys, Part II: Modeling of Polycrystals, *Mech. Mater.*, 2006, **38**, p 391–429
4. P. Popov and D.C. Lagoudas, A 3-D Constitutive Model for Shape Memory Alloys Incorporating Pseudoelasticity and Detwinning of Self-Accommodated Martensite, *Int. J. Plasticity*, 2007, **23**, p 1679–1720
5. V.I. Levitas, Thermomechanical Theory of Martensitic Phase Transformations in Inelastic Materials, *Int. J. Solids Struct.*, 1998, **35**, p 889–940
6. B. Peultier, T. Ben Zineb, and E. Patoor, Macroscopic Constitutive Law for SMA: Application to Structure Analysis by FEM, *Mater. Sci. Eng. A*, 2006, **438–440**, p 454–458
7. B. Raniecki and Ch. Lexcellent, R_L Models of Pseudoelasticity and Their Specification for Some Shape-Memory Solids, *Eur. J. Mech. A Solids*, 1994, **13**, p 21–50
8. S. Reese and D. Christ, Finite Deformation Pseudo-Elasticity of Shape Memory Alloys—Constitutive Modeling and Finite Element Implementation, *Int. J. Plasticity*, 2008, **24**, p 455–482
9. A.C. Souza, E.N. Mamiya, and N. Zouain, Three-Dimensional Model for Solids Undergoing Stress-Induced Phase Transformations, *Eur. J. Mech. A: Solids*, 1998, **17**, p 789–806
10. F. Auricchio and L. Petrini, A Three-Dimensional Model Describing Stress-Temperature Induced Solid Phase Transformations: Solution Algorithm and Boundary Value Problems, *Int. J. Numer. Methods Eng.*, 2004, **61**, p 807–836
11. F. Auricchio, A. Reali, and U. Stefanelli, A Macroscopic 1D Model for Shape Memory Alloys Including Asymmetric Behaviors and Transformation-Dependent Elastic Properties, *Comput. Methods Appl. Mech. Eng.*, 2009, **198**, p 1631–1637
12. F. Auricchio and A. Reali, A Phenomenological One-Dimensional Model Describing Stress-Induced Solid Phase Transformation with Permanent Inelasticity, *Mech. Adv. Mater. Struct.*, 2007, **14**, p 43–55
13. F. Auricchio, A. Reali, and U. Stefanelli, A Three-Dimensional Model Describing Stress-Induced Solid Phase Transformation with Permanent Inelasticity, *Int. J. Plasticity*, 2007, **23**, p 207–226
14. F. Auricchio and L. Petrini, A Three-Dimensional Model Describing Stress-Temperature Induced Solid Phase Transformations: Thermomechanical Coupling and Hybrid Composite Applications, *Int. J. Numer. Methods Eng.*, 2004, **61**, p 716–737